

# Understanding from First-Principles Why $\text{LiNH}_2\text{BH}_3 \cdot \text{NH}_3\text{BH}_3$ Shows Improved Dehydrogenation over $\text{LiNH}_2\text{BH}_3$ and $\text{NH}_3\text{BH}_3$

Wen Li,<sup>†</sup> Ralph H. Scheicher,<sup>‡</sup> C. Moysés Araújo,<sup>‡</sup> Guotao Wu,<sup>§</sup> Andreas Blomqvist,<sup>‡</sup> Chenzhang Wu,<sup>§</sup> Rajeev Ahuja,<sup>‡</sup> Yuan Ping Feng,<sup>†</sup> and Ping Chen<sup>\*,§</sup>

Dalian Institute of Chemical Physics, Chinese Academy of Sciences, 116023, People's Republic of China, Department of Physics, National University of Singapore, 117542, Singapore, and Condensed Matter Theory Group, Department of Physics and Astronomy, Box 516, Uppsala University, SE-751 20 Uppsala, Sweden

Received: April 25, 2010; Revised Manuscript Received: September 4, 2010

Lithium amidoborane–ammonia borane ( $\text{LiNH}_2\text{BH}_3 \cdot \text{NH}_3\text{BH}_3$ ,  $\text{LiAB} \cdot \text{AB}$  for short) was synthesized recently. Compared with lithium amidoborane ( $\text{LiNH}_2\text{BH}_3$ ,  $\text{LiAB}$  for short) and ammonia borane ( $\text{NH}_3\text{BH}_3$ ,  $\text{AB}$  for short), this new ammonia borane derivative has better dehydrogenation kinetics and releases 14.8 wt % hydrogen with peak temperatures at ca. 80 and 140 °C, respectively. In this report, first-principles calculations were employed to reveal the differences in dehydrogenation properties of  $\text{AB}$ ,  $\text{LiAB}$ , and  $\text{LiAB} \cdot \text{AB}$ . Furthermore, we attempted to correlate the crystal structure and electronic properties with dehydrogenation performance. The results show that  $\text{Li}^+$  cations play similar roles in  $\text{LiAB} \cdot \text{AB}$  as in  $\text{LiAB}$  in destabilizing the B–H and N–H bonds, and the mechanism of the first-step dehydrogenation of  $\text{LiAB} \cdot \text{AB}$  is likely via the dissociation and combination of hydridic  $\text{H}^\delta-$ (B) from  $\text{LiAB}$  molecule and protonic  $\text{H}^\delta+(N)$  from the adjacent  $\text{AB}$  molecule, rather than from the  $[\text{LiAB}]$  or  $[\text{AB}]$  layer alone, resulting in the desorption of  $\text{H}_2$  at lower temperatures.

## 1. Introduction

Ammonia borane ( $\text{NH}_3\text{BH}_3$ ,  $\text{AB}$  for short) has attracted considerable attention as a hydrogen storage material in the past few years because of its high hydrogen storage capacity (19.6 wt %).<sup>1</sup> However, the relatively poor kinetics and high temperature of dehydrogenation as well as issues with energetically undesirable regeneration of the system are still big challenges for the practical application of  $\text{AB}$  as a useful hydrogen storage material.<sup>2–4</sup> Moreover, borazine as a volatile byproduct of dehydrogenation of  $\text{AB}$  can poison polymer electrolyte membrane (PEM) fuel cells.<sup>5</sup> Various approaches have been developed to improve the performance of  $\text{AB}$ .<sup>2,6–8</sup> One such approach is substituting one H atom in the  $[\text{NH}_3]$  unit by an alkali metal or alkaline earth element to form metal amidoboranes such as  $\text{LiNH}_2\text{BH}_3$ <sup>9–14</sup> ( $\text{LiAB}$  for short),  $\text{NaNH}_2\text{BH}_3$ <sup>10,14,15</sup> ( $\text{NaAB}$  for short), or  $\text{Ca}(\text{NH}_2\text{BH}_3)_2$ <sup>12,16,17</sup> ( $\text{CaAB}$  for short). It was shown experimentally that these alkali or alkaline earth metal amidoboranes release hydrogen under milder conditions with considerable suppression of unwanted gaseous byproducts. Recent experimental and theoretical studies on  $\text{LiAB}$  and  $\text{NaAB}$  revealed that ionic bonds are formed between the metal and  $\text{NH}_2\text{BH}_3$  unit.<sup>12,18–20</sup> As  $\text{NH}_2\text{BH}_3$  attracts electron from metal, the reactivity of hydridic B–H bond in metal amidoboranes can be enhanced. Moreover, the charged  $[\text{NH}_2\text{BH}_3]^-$  ions create polar reaction environment, which facilitates  $\text{BH} \cdots \text{HN}$  interactions between the adjacent units.<sup>12,18–20</sup> As a consequence, lower dehydrogenation temperatures in the alkali metal amidoboranes (~90 °C for  $\text{LiAB}$  and  $\text{NaAB}$ ) can be achieved compared with that of pristine  $\text{AB}$  (~110 °C).

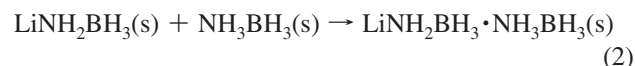
\* Corresponding author: E-mail pchen@dicp.ac.cn; tel (+86) 411 84379583.

<sup>†</sup> National University of Singapore.

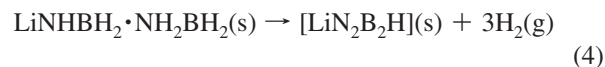
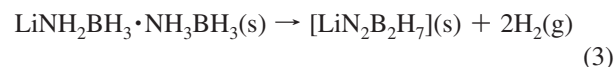
<sup>‡</sup> Uppsala University.

<sup>§</sup> Chinese Academy of Sciences.

More recently, a new ammonia borane derivative was formed through reaction of  $\text{LiH}$  with two  $\text{AB}$  or reaction of  $\text{LiAB}$  with  $\text{AB}$  as described by the following reactions:<sup>21</sup>



This new compound, lithium amidoborane–ammonia borane,  $\text{LiNH}_2\text{BH}_3 \cdot \text{NH}_3\text{BH}_3$  ( $\text{LiAB} \cdot \text{AB}$  for short), has a hydrogen storage capacity of 14.8 wt % and a lower dehydrogenation temperature (onset at 58 °C and first peak at 80 °C) as compared to  $\text{AB}$  and  $\text{LiAB}$ . Moreover, borazine is undetected. It was proposed that dehydrogenation of  $\text{LiAB} \cdot \text{AB}$  follows a two-step process:



Synchrotron X-ray diffraction characterization shows that the crystal structure of  $\text{LiAB} \cdot \text{AB}$  consists of alternate layers of  $[\text{LiNH}_2\text{BH}_3]$  ( $[\text{LiAB}]$ ) and  $[\text{NH}_3\text{BH}_3]$  ( $[\text{AB}]$ ) molecules, in which the  $\text{Li}^+$  bonds with  $[\text{NH}_2\text{BH}_3]^-$  anion and is also coordinated with  $\text{H}^\delta-$  in the  $\text{NH}_3\text{BH}_3$  molecule with a distance in the range of 1.953–2.165 Å.<sup>21</sup> Such a  $\text{Li}^+$  coordination environment is likely to weaken the dihydrogen bonds, resulting in a less stable  $\text{LiAB} \cdot \text{AB}$ .

There have been several first-principles studies on  $\text{AB}$ <sup>19,22–30</sup> and  $\text{LiAB}$ <sup>12,18,19,31–33</sup> in the past to determine the structures and

decomposition pathways and to understand the improved dehydrogenation performance. In this study, we employed first-principles calculations based on density functional theory (DFT) to investigate the crystal and electronic structures and energetics of H atom desorption of solid LiAB $\cdot$ AB. Our results show that Li $^{+}$  cations destabilize H atoms in an efficient way in LiAB $\cdot$ AB due to the alternate [LiAB] $\cdot$ [AB] layered structure. With weaker B–H and N–H bonds, in the first step of dehydrogenation of LiAB $\cdot$ AB, the dissociation and combination of an H $^{+}$ (B) atom from a LiAB molecule and an H $^{+}$ (N) atom from the adjacent AB molecule, become energetically favorable, which could explain the lower dehydrogenation temperature of LiAB $\cdot$ AB compared with those of AB and LiAB. For convenience, we denote AB, LiAB, and LiAB $\cdot$ AB as **I**, **II**, and **III**, respectively, in the following discussion.

## 2. Computational Methods

Calculations were carried out within the framework of density functional theory<sup>34</sup> by the projector-augmented wave (PAW) method<sup>35</sup> and the generalized gradient approximation (GGA)<sup>36</sup> for the exchange–correlation energy functional, as implemented in the Vienna ab initio simulation package (VASP).<sup>37</sup> The GGA calculation was performed with the Perdew–Wang 91 exchange–correlation potential. CaAB (**I**) has orthorhombic structure with space group  $Pmn_2_1$  while **II** and **III** crystallize into tetragonal structures with space groups  $Pbca$  and  $P21/C$ , respectively. The unit cells of **I**, **II**, and **III** contain 16, 64, and 64 atoms, respectively. We first calculated the equilibrium lattice parameters using a plane-wave cutoff energy of 520 eV and a  $5 \times 5 \times 5$   $k$ -point mesh in the Monkhorst–Pack scheme.<sup>38</sup> The geometry optimization has been done by minimizing the Hellmann–Feynman forces on the atoms and stresses on the unit cell without any symmetry constraint. In all calculations, self-consistency was achieved with a tolerance in total energy of 0.01 meV, and atomic forces were converged to less than 0.01 eV/Å. The optimized lattice parameters of **I**, **II**, and **III** are in reasonable agreement with available experimental values (see Tables S1, S2, and S3 in Supporting Information). Figure 1 shows the unit cells of **I**, **II** and **III**. The structure of **III** consists of alternate [LiAB] and [AB] layers along [100] direction. The subsequent calculations were performed in  $2 \times 2 \times 2$ ,  $1 \times 2 \times 1$ , and  $1 \times 1 \times 2$  supercells of **I**, **II**, and **III** systems, respectively, with an energy cutoff of 520 eV and  $4 \times 4 \times 4$   $k$ -point mesh employed. The electronic properties were analyzed via the electron localization function (ELF)<sup>39</sup> and the electronic densities of states (DOS), which were calculated by means of the modified tetrahedron Blöchl methods.<sup>40</sup>

## 3. Results and Discussion

**3.1. Electronic Density of States.** The calculated partial density of states (DOS) for **I**, **II**, and **III** are shown in Figure 2. In general, they have a finite energy gap and therefore they exhibit nonmetallic features. The calculated GGA band gap ( $E_g$ ) of **III** (4.6 eV) is slightly greater than that of **II** (4.2 eV), and both of these ammonia borane derivatives have narrower band gaps than that of solid **I** (6 eV). The actual gap could be even larger since density functional theory is known to underestimate the band gap of semiconductors and insulators. The total DOS for **I**, **II**, and **III** comprises three well-separated regions: region A, below  $-1$  eV (lower energy region of valence band); region B, from  $-1$  to  $0$  eV (top of valence band); and region C, above  $4$  eV (conduction band).

In DOS of **III** (Figure 2a,b), the lowest energy part (from  $-7.3$  to  $-8.3$  eV) of region A is mainly due to N p-states, H(N)

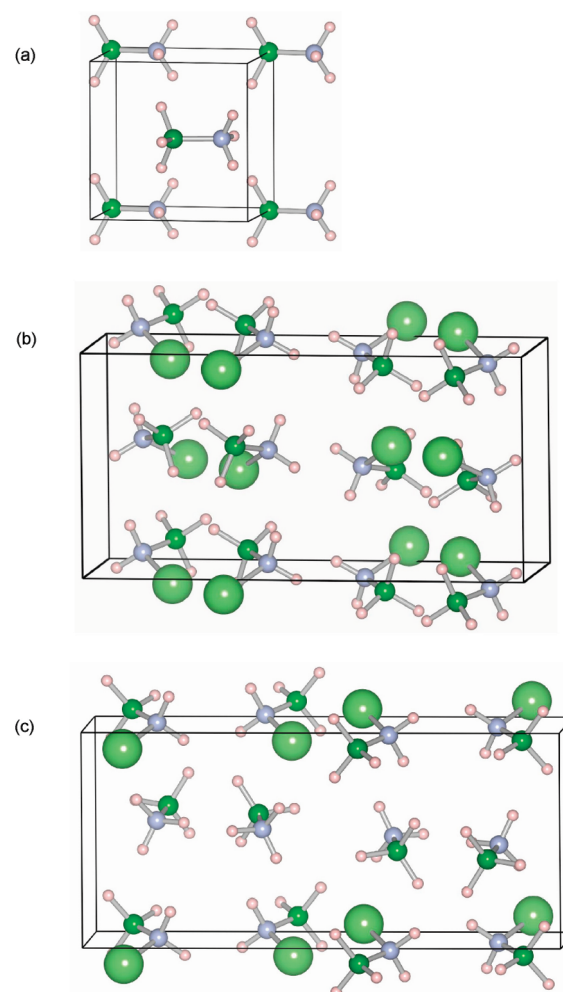


**Figure 1.** Unit cells of solid (a) AB, (b) LiAB and (c) LiAB $\cdot$ AB. Large green, small light blue, small green, and small pink spheres denote Li, N, B, and H atom, respectively.

s-states [H(N) denotes H bonded to N], and B s-states from the AB molecule. The neighbor area (from  $-6.5$  to  $-7.3$  eV) is due to N p-states and B s-states from the LiAB molecule. The sharp peaks around  $-5.8$  eV are contributed by one N p-state and two H(N) s-states from the LiAB molecule. Almost all elements in both LiAB and AB molecules contribute to the electronic densities in the area from  $-3.5$  to  $-4.7$  eV, while in the higher energy area from  $-1.4$  to  $-3.0$  eV, B p-states and H(B) s-states [H(B) denotes H bonded to B] are obviously involved, and a small contribution also comes from Li atom. The total electronic density in region B which covers the top of the valence band, are mainly attributed to N p-states, B p-states, and H(B) s-states, with only small contributions from Li s- and p-states. The broad peaks in the conduction band in region C mainly originate from Li s- and p-states; B and N atoms are also minor contributors to the electronic density in the conduction band (notice the different y-axis scales of partial DOS of B, N, and Li atoms). The above analyses suggest the following: (i) The covalent features of N–H and B–H are due to the strong sp hybridization between N and H(N) and between B and H(B) in the valence band; the N–H bond is generally stronger than the B–H bond, as the overlap region of N p-states and H(N) s-states is energetically lower than that of B p-states and H(B) s-states. (ii) Hybridization on the valence band between Li and H(B) atoms could be regarded as an indication of covalent coordination bond. (iii) The interaction character

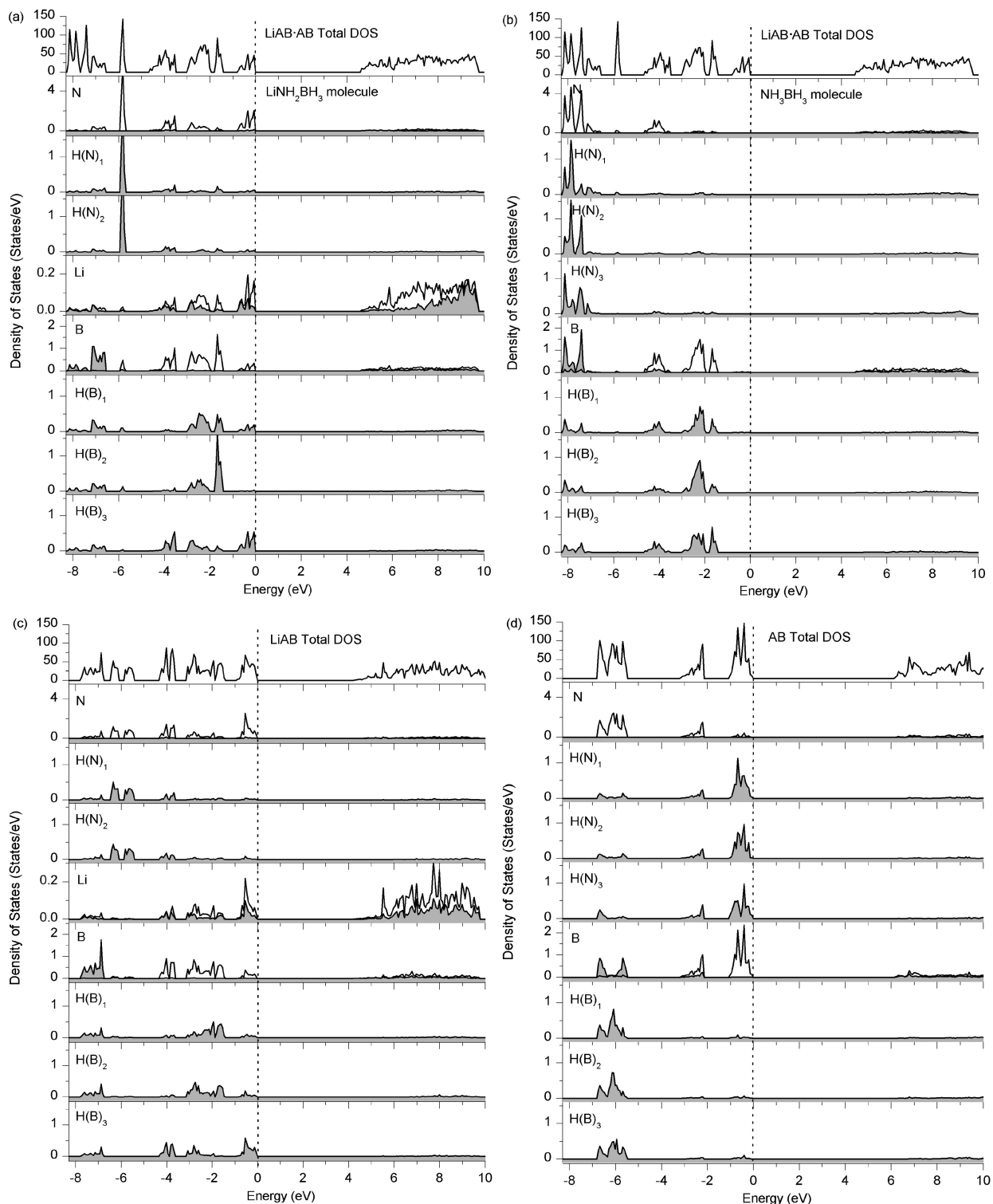


**Figure 2.** Total and partial electronic density of states (DOS) of (a)  $\text{LiNH}_2\text{BH}_3$  molecule in  $\text{LiAB} \cdot \text{AB}$ , (b)  $\text{NH}_3\text{BH}_3$  molecule in  $\text{LiAB} \cdot \text{AB}$ , (c)  $\text{LiAB}$ , and (d)  $\text{AB}$ . The Fermi level is set at zero energy and marked by vertical dotted lines; s-electron contributions are depicted with gray shading, and p-states are denoted as solid lines.

between Li and N atoms is essentially ionic, also with a partial covalent bonding feature from their overlapping of electron densities in the valence band.

When the partial DOS of the  $\text{LiAB}$  molecule of **III** is compared with that of **II**, the prompted N p-peak in the  $\text{LiAB}$  molecule indicates that the N atom attracts more electrons from  $\text{Li}^+$  cation, which is in response to the relative lower Li p-states in the conduction band of **III**; thus the more charged N results in a stronger B–N hybridization. This alteration also leads the

B–H bond in the  $\text{LiAB}$  molecule of **III** to be more reactive and provides a more polar reaction environment for dihydrogen interaction. The N p-state, B p-state, and H s-state of AB molecule of **III** display a left shift comparing with the partial DOS of **I**, suggesting that both B–H and N–H bonds in the AB molecule are generally stronger than that in **I**.

**3.2. Charge Density and Electron Localization Function.** To get a better insight into the chemical bonding of these compounds, we have analyzed charge density distribution and

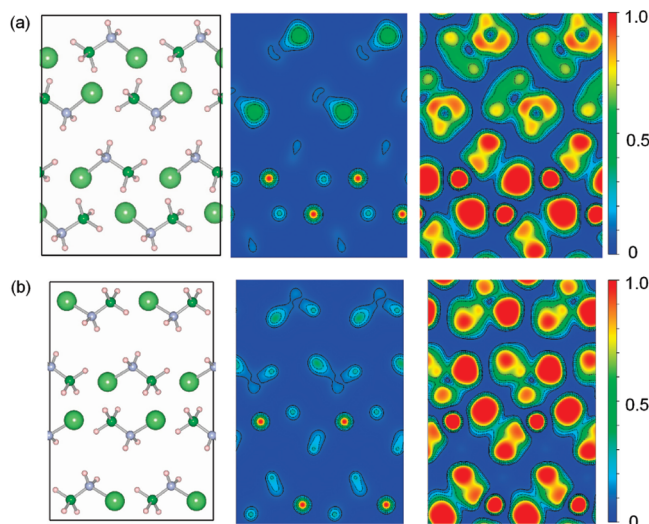


**Figure 3.** Charge density distribution (middle panel) in (a) (100) plane in LiAB and (b) (100) plane in LiAB·AB. Left and right panels display the atomic motif and ELF contour plot in the selected planes, with color bar scalar (ELF approaching 1 implies a covalent bond or lone pair; an ELF value around 0.5 denotes uniform density distribution and free electron gas phase; ELF approaching 0 indicates the absence of electrons, such as an ionic bond). Large green, small light blue, small green, and small pink spheres denote Li, N, B, and H atom, respectively.

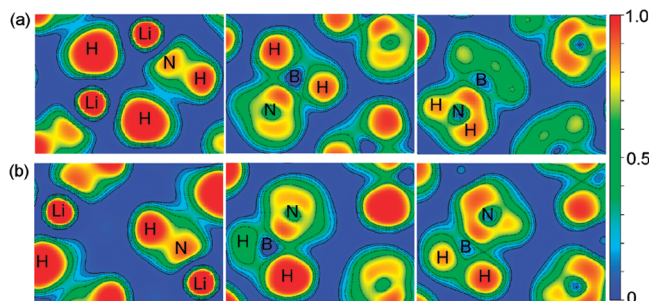


**Figure 4.** (a) Partial ELF contour plots in the LiAB cell of (100) plane passing through Li atoms (left panel), B atoms (middle panel), and N atoms (right panel). (b) Partial ELF contour plots in the LiAB·AB cell of (100) plane passing through Li (left panel), B (middle panel), and N (right panel) atoms.

electron localization function (ELF). In Figure 3, the middle panels show calculated valence-charge densities within the (100) plane of **II** and **III**; the left and right panels present the atomic motif and ELF plot in the same plane. The ELF is not a direct measure of electron density but can be associated with electron density in most cases, since ELF represents a continuous and differentiable scalar field in three-dimensional space and so does the electron density.<sup>41</sup> Near the Li, N, and H sites, high charge density is observed in the immediate vicinity of the nuclei. The predominant covalent nature of the bonding between N and H and between B and H is confirmed by the finite charge density between these atoms. The electron distribution between Li<sup>+</sup> and the [NH<sub>2</sub>BH<sub>3</sub>]<sup>-</sup> is almost zero, an indication of ionic-type interaction between Li<sup>+</sup> and [NH<sub>2</sub>BH<sub>3</sub>]<sup>-</sup>.

Partial ELF contour plots of the selected planes are shown in Figure 4. In the left panel, a high ELF value on the Li<sup>+</sup> cations implies the highly localized s-electrons; a nearly spherical structure of the ELF around the nuclei separated by a region with a very low ELF value is characteristic of ionic bonds, which are found around Li<sup>+</sup> cations and within the interstitial regions between Li<sup>+</sup> and [NH<sub>2</sub>BH<sub>3</sub>]<sup>-</sup> units, indicative of ionic Li—N bonds, whereas the B atoms are slightly polarized (middle

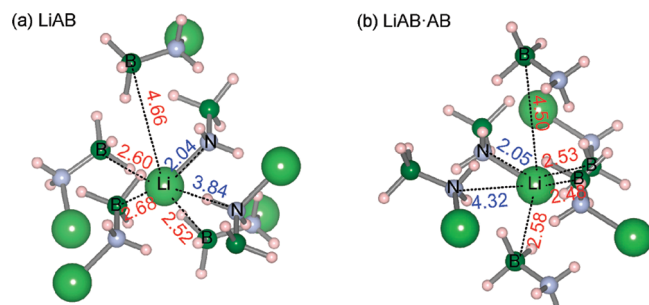


**Figure 5.** Coordination environment of Li<sup>+</sup> in (a) LiAB and (b) LiAB·AB. The distance between Li and B atoms, between Li and N atoms are denoted in red and blue, respectively, units in angstroms. Large green, small light blue, small green, and small pink spheres denote Li, N, B and H atom, respectively.

panel), as the contours in the ring holes are not circular, but triangular in shape, due to the repulsive interaction with the negatively charged H atoms. High electron localization is seen in the region between adjacent B and N atoms, which reflects the covalent nature of B—N dative bond.

**3.3. Chemical Bond Lengths.** The coordination environments of Li<sup>+</sup> in **II** and in **III** are displayed in Figure 5. In **II**, Li<sup>+</sup> is connected with one [NH<sub>2</sub>BH<sub>3</sub>]<sup>-</sup> unit and surrounded by three BH<sub>3</sub> units, with Li<sup>+</sup>—B distances in the range 2.52–2.68 Å. In **III**, Li<sup>+</sup> is connected with one [NH<sub>2</sub>BH<sub>3</sub>]<sup>-</sup> unit and surrounded by three BH<sub>3</sub> units with Li<sup>+</sup>—B distances in the range 2.48–2.58 Å. Generally, the distance between Li<sup>+</sup> and the surrounding B atoms in **III** is shorter than in **II**. Moreover, the shortest Li<sup>+</sup>—H<sup>δ-</sup>(B) distances (1.95 Å between two neighboring LiAB molecules and 1.96 Å between LiAB and AB molecules) in **III** are also slightly smaller than the shortest distance of Li<sup>+</sup>—H<sup>δ-</sup>(B) (1.97 Å) in **II** (not shown in Figure 5 but listed in Table 1). From the coordination environment of Li<sup>+</sup>, we can see that the configuration of **III** is more compact than that of **II**, and H(B) atoms in both LiAB and AB molecules of **III** coordinate with Li<sup>+</sup>.

The calculated lengths of B—N, B—H, and N—H bonds and the distances H<sup>δ-</sup>(B)…H<sup>δ+</sup>(N) are listed in Table 1. In **III**, the B—N bond length of 1.55 Å in the LiAB molecule and 1.59 Å in the AB molecule are almost the same as the B—N bond lengths in solid **II** (1.55 Å) and solid **I** (1.59 Å). The mean B—H and N—H bond lengths in the LiAB and AB molecules of **III** are also similar to those in solid **I** and **II**.

The distance of H<sup>δ-</sup>(B)…H<sup>δ+</sup>(N) is one of the characteristic parameters for the crystal stability of AB-based compounds.<sup>12</sup> In **III**, there are three kinds of H<sup>δ-</sup>(B)…H<sup>δ+</sup>(N) distances: (i) H<sub>i</sub><sup>δ-</sup>(B)…H<sub>i</sub><sup>δ+</sup>(N) is the distance between two hydrogen atoms in two adjacent LiAB molecules within the [LiAB] layers, (ii) H<sub>ii</sub><sup>δ-</sup>(B)…H<sub>ii</sub><sup>δ+</sup>(N) is the distance between two adjacent AB molecules within the [AB] layers, and (iii) H<sub>i</sub><sup>δ-</sup>(B)…H<sub>ii</sub><sup>δ+</sup>(N) is the distance between a LiAB molecule and an adjacent AB molecule. The shortest distances in **III** are (i) 2.65, (ii) 1.90, and (iii) 1.98 Å, respectively. H<sub>i</sub><sup>δ-</sup>(B)…H<sub>i</sub><sup>δ+</sup>(N)<sub>min</sub> (2.65 Å) is longer than the sum of van der Waals radii (2.4 Å), evidencing the vanishing of dihydrogen bonding, and this distance is longer than the shortest dihydrogen distance of 2.32 Å between two LiAB molecules in solid **II**. H<sub>ii</sub><sup>δ-</sup>(B)…H<sub>ii</sub><sup>δ+</sup>(N)<sub>min</sub> (1.90 Å) is also longer than the shortest dihydrogen bond distance of 1.878 Å in solid **I**. Thus the H<sup>δ-</sup>(B)…H<sup>δ+</sup>(N) interactions in **III** are weaker in both the [LiAB] layers and the [AB] layers, resulting in the crystal lattice of **III** being less stable than those of **II** and **I**, which is also supported by evidence of differential scanning calorimetry (DSC) measurement that the onset melting

**TABLE 1:** Selected Calculated Interatomic Distances in LiAB, LiAB·AB, and AB<sup>a</sup>

distance	LiAB (II)	LiAB·AB (III)			AB (I)
		(i) within LiAB molecule	(ii) within AB molecule	(iii) between LiAB and AB molecules	
$\text{Li}^+ \cdots \text{H}^\delta-(\text{B})_{\min}$ (Å)	1.97	1.95 <sup>b</sup>		1.96 <sup>c</sup>	
B–N (Å)	1.55 [1.561] <sup>12</sup>	1.55 [1.559] <sup>21</sup>	1.59 [1.609] <sup>21</sup>		1.59 [1.58] <sup>43</sup>
B–H <sub>mean</sub> (Å)	1.24	1.24 [1.23] <sup>21</sup>	1.22 [1.23] <sup>21</sup>		1.22 [1.18] <sup>43</sup>
N–H <sub>mean</sub> (Å)	1.02 [1.025] <sup>12</sup>	1.02 [1.03] <sup>21</sup>	1.03 [1.04] <sup>21</sup>		1.03 [1.07] <sup>43</sup>
$\text{H}^\delta-(\text{B}) \cdots \text{H}^{\delta+}(\text{N})_{\min}$ (Å)	2.32	2.65 <sup>d</sup>	1.90 <sup>e</sup>	1.98 <sup>f</sup>	1.88 [1.7] <sup>44</sup>
$\text{f} \text{H}_i^\delta-(\text{B}) \cdots \text{H}_{ii}^{\delta+}(\text{N})$					

<sup>a</sup> Available experimental data are shown in brackets. <sup>b</sup>  $\text{Li}_i^+ \cdots \text{H}_i^\delta-(\text{B})$ . <sup>c</sup>  $\text{Li}_i^+ \cdots \text{H}_{ii}^\delta-(\text{B})$ . <sup>d</sup>  $\text{H}_i^\delta-(\text{B}) \cdots \text{H}_i^{\delta+}(\text{N})$ . <sup>e</sup>  $\text{H}_{ii}^\delta-(\text{B}) \cdots \text{H}_{ii}^{\delta+}(\text{N})$ .

**TABLE 2:** Hydrogen Removal Energies of AB, LiAB, and LiAB·AB<sup>a</sup>

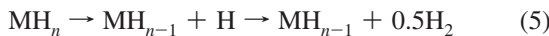
LiAB (II)	LiAB·AB (III)			AB (I)
	LiAB molecule	AB molecule	AB (I)	
$\Delta E_{\text{H}(\text{B})}$ (eV)	2.05	1.99	2.42	2.32
$\Delta E_{\text{H}(\text{N})}$ (eV)	2.59	2.49	2.37	2.54

<sup>a</sup> Hydrogen removal energy ( $\Delta E_{\text{H}}$ ) is calculated as  $\Delta E_{\text{H}} = E_{\text{coh}}[\text{MH}_{n-1}] + 0.5E_{\text{coh}}[\text{H}_2] - E_{\text{coh}}[\text{MH}_n]$ , in which  $[\text{MH}_n]$  denotes the solid system contains  $n$  hydrogen atoms.

temperature of **III** (58 °C) is lower than those of **II** (82 °C) and **I** (95 °C). The relatively shorter dihydrogen bond  $\text{H}^\delta-(\text{B}) \cdots \text{H}_{ii}^{\delta+}(\text{N})$  (1.98 Å) could lead to the detachment and consequent combination of  $\text{H}^\delta-$  and  $\text{H}^{\delta+}$  occur between the [LiAB] and the [AB] layers, rather than within the [LiAB] or [AB] layer alone, which we will elaborate below.

**3.4. Hydrogen Removal Energies.** The strength of hydrogen–host bonds can be quantified by the change in enthalpy before and after the dissociation of hydrogen atom from the system,<sup>26</sup> which is also a qualitative indicator of the temperature for releasing hydrogen from the system,<sup>42</sup> so we further calculated the energy cost to remove a hydrogen atom from **I**, **II**, and **III**, respectively. The H atom that has the longest bond distance with B or N in each solid structure is chosen to be removed. The H atoms associated with LiAB and AB molecules in **III** were considered separately. The atomic coordinates of the structure with one hydrogen atom removed were fully reoptimized.

In view of the fact that hydrogen atoms are desorbed associatively, forming a hydrogen molecule, we specify the hydrogen atom removal occurred as the following reaction:



in which  $\text{MH}_n$  denotes the solid system contains  $n$  hydrogen atom, and thus hydrogen atom removal energy should be defined as

$$\Delta E_{\text{H}} = E_{\text{coh}}[\text{MH}_{n-1}] + 0.5E_{\text{coh}}[\text{H}_2] - E_{\text{coh}}[\text{MH}_n] \quad (6)$$

where  $E_{\text{coh}}$  is the cohesive energy, the difference between the electronic total energy of the atoms of a solid and the sum of the total energy of individual free atoms.

The calculated hydrogen removal energies are listed in Table 2. Generally it costs less energy to remove the  $\text{H}^\delta-(\text{B})$  atom than to remove the  $\text{H}^{\delta+}(\text{N})$  atom, which indicates the breaking of the B–H bond is prior to the dissociation of N–H bond in the initial state of dehydrogenation of **I**, **II**, and **III**. The  $\text{H}^\delta-(\text{B})$

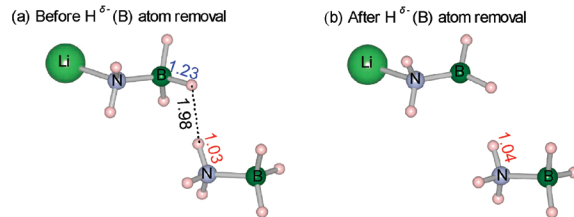


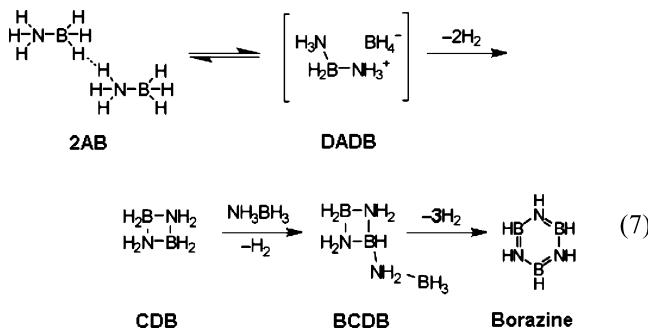
**Figure 6.** Derived LiAB molecule and adjacent AB molecule from the optimized solid structure of LiAB·AB (a) before and (b) after removal of one  $\text{H}^\delta-(\text{B})$  atom. Large green, small light blue, small green, and small pink spheres denote Li, N, B and H atom, respectively.  $\text{H}^\delta-\cdots \text{H}^{\delta+}$  dihydrogen bond lengths and the associated  $\text{B}-\text{H}^\delta-$  and  $\text{N}-\text{H}^{\delta+}$  bond lengths are denoted in black, blue and red, respectively. All bond lengths are given in angstroms.

atom removal energy of 1.99 eV from the LiAB molecule of solid **III** is slightly less than that of 2.05 eV from solid **II**, but such a small difference (0.06 eV) is virtually insignificant and thus these two removal energies can be regarded as being essentially equal; whereas 1.99 eV is much lower than the  $\text{H}^\delta-(\text{B})$  atom removal energy of 2.32 eV from solid **I**. However, energy of 2.42 eV is needed to remove the  $\text{H}^\delta-(\text{B})$  atom from the AB molecule of **III**, which is higher than the values for solid **I** and **II**. The  $\text{H}^{\delta+}(\text{N})$  atom removal energy from the AB molecule of **III** is 2.37 eV, about 0.2 eV less than that of 2.54 eV from solid **I** and that of 2.59 eV from solid **II**, while the  $\text{H}^{\delta+}(\text{N})$  atom removal energy from the LiAB molecule of **III** is 2.49 eV. From the above comparison, we can see that breaking of the  $\text{B}-\text{H}^\delta-$  bond in the LiAB molecule and breaking of the  $\text{N}-\text{H}^{\delta+}$  bond in the AB molecule of solid **III** carry less energy cost than those in solid **I** and **II**.

**3.5. Dehydrogenation Mechanism of LiAB·AB.** The above analyses could shine a light on the dehydrogenation mechanism of **III**. It takes less energy to remove  $\text{H}^\delta-(\text{B})$  from the LiAB molecule and  $\text{H}^\delta-(\text{N})$  from the AB molecule, indicating that these atoms are easier to dissociate from the solid **III**, so the intermolecular dehydrogenation between the [LiAB] layer and the [AB] layer is likely the main course in the first-step dehydrogenation. It is also noted that  $\text{H}^\delta-(\text{B})$  in the LiAB molecule forms a short dihydrogen bond (with a length of 1.98 Å) with  $\text{H}^{\delta+}(\text{N})$  in the adjacent AB molecule. Because the dissociation of  $\text{H}^\delta-(\text{B})$  occurs prior to that of  $\text{H}^{\delta+}(\text{N})$ , we also examined the reoptimized structure after removal of  $\text{H}^\delta-(\text{B})$  in **III**. It was found that after removal of  $\text{H}^\delta-(\text{B})$ , the nearby associated  $\text{N}-\text{H}^{\delta+}$  bond becomes the longest N–H bond in the optimized solid structure (see Figure 6), which indicates that this  $\text{H}^{\delta+}(\text{N})$  atom will be easier to further detach from the system than other  $\text{H}^{\delta+}(\text{N})$  atoms, and to subsequently combine with the previous detached  $\text{H}^\delta-(\text{B})$  atom to form the  $\text{H}_2$  molecule. Therefore, we can attribute the mechanism of first-step dehydrogenation of **III** to the dissociation of  $\text{H}^\delta-(\text{B})$  atom from the LiAB molecule and  $\text{H}^{\delta+}(\text{N})$  atom from the AB molecule to form the first  $\text{H}_2$  molecule.

The initiation of dehydrogenation of BNH-containing chemical hydride systems needs to overcome a kinetic barrier, which is related to the energy cost for the breaking of B–H and N–H bonds and formation of H<sub>2</sub>. Thus the hydrogen removal energy may reflect partially the kinetic aspect of the dehydrogenation. Previous experimental and theoretical studies on **I**<sup>25,42</sup> and **II**<sup>18,31,33</sup> indicated that the initial state of dehydrogenation is controlled by the break-up of the B–H bond, which is regarded as the rate-limiting step. So, the experimental fact that **III** starts to release H<sub>2</sub> at a lower temperature than **I** and **II** can be explained satisfactorily by the smaller H<sup>δ−</sup>(B) atom removal energy in **III** (1.99 eV) than those of **I** (2.32 eV) and **II** (2.05 eV).

Finally, we address the issue of suppression of borazine in **III**. Borazine (B<sub>3</sub>N<sub>3</sub>H<sub>6</sub>) as the byproduct of **I** is one of the drawbacks for the PEM fuel cell application. The formation of borazine from **I** was proposed as<sup>1,5,30,42</sup>



The initial step is isomerization of AB to DADB (diammoniate of diborane, [NH<sub>3</sub>BH<sub>2</sub>NH<sub>3</sub>]<sup>+</sup>[BH<sub>4</sub>]<sup>-</sup>) and then DADB cyclizes to CDB (cyclodiborazane, *c*-B<sub>2</sub>N<sub>2</sub>H<sub>8</sub>) in a subsequent reaction. CDB reacts with AB to form the new species BCDB (*B*-(cyclodiborazanyl)aminoborohydride, cyc[NH<sub>2</sub>BH<sub>2</sub>NH<sub>2</sub>BH]-NH<sub>2</sub>BH<sub>3</sub>), and the further dehydrogenation of BCDB generates borazine. We can see that the generation of borazine relies on the formation of intermediate DADB between two neighboring AB molecules and then the cyclization of BH<sub>2</sub>–NH<sub>2</sub> units. Although there are AB molecules in **III**, the intermolecular dehydrogenation mechanism between LiAB and AB molecules could prevent the dehydrogenation occurring within the [AB] layer alone, without the formation of DADB and CDB, so the formation of borazine is consequently avoided.

#### 4. Conclusions

In this study, theoretical calculations were carried out on the newly developed lithium amidoborane–ammonia borane (LiNH<sub>2</sub>BH<sub>3</sub>•NH<sub>3</sub>BH<sub>3</sub>, LiAB•AB for short) system. Electronic density of states and electron localization function analyses indicate the covalent bond nature of N–H and B–H bonds but ionic bonding between Li and N. Bond length analyses show that LiAB•AB possesses weakened H<sup>δ−</sup>(B)…H<sup>δ+</sup>(N) interactions both within the [LiAB] layers and within the [AB] layers, resulting in a lower stability of LiAB•AB as compared to solid LiAB and AB. Analyses of B–H and N–H bond lengths combined with hydrogen removal energy calculations reveal that the first-step dehydrogenation is via the combination of H<sup>δ−</sup>(B) atom from the LiAB molecule and H<sup>δ+</sup>(N) atom from the AB molecule in LiAB•AB, resulting in the desorption of H<sub>2</sub> at lower temperature.

**Acknowledgment.** We acknowledge financial support from Hundred Talents Project and Knowledge Innovation Program

of Chinese Academy of Sciences (KGCX2-YW-806 and KJCX2-YW-H21) and 973 Project (2010CB631304), the National Natural Science Foundation of China (No. 20971120, 10979051 and 20973162), the National University of Singapore, and STINT, as well as from the Swedish Research Council (VR) and Wenner-Gren Foundations. We are also grateful to SNIC and UPPMAX for providing computing time.

**Supporting Information Available:** Three tables as described in the text. This material is available free of charge via the Internet at <http://pubs.acs.org>.

#### References and Notes

- Stephens, F. H.; Pons, V.; Tom Baker, R. *Dalton Trans.* **2007**, 2613.
- Gutowska, A.; Li, L.; Shin, Y.; Wang, C. M.; Li, X. S.; Linehan, J. C.; Smith, R. S.; Kay, B. D.; Schmid, B.; Shaw, W.; Gutowski, M.; Autrey, T. *Angew. Chem., Int. Ed.* **2005**, *44*, 3578.
- Stephens, F. H.; Pons, V.; Baker, R. T. *Dalton Trans.* **2007**, 2613.
- Marder, T. B. *Angew. Chem., Int. Ed.* **2007**, *46*, 8116.
- Nutt, W. R.; McKee, M. L. *Inorg. Chem.* **2007**, *46*, 7633.
- Clark, T. J.; Manners, I. *J. Organomet. Chem.* **2007**, *692*, 2849.
- Neiner, D.; Karkamkar, A.; Linehan, J. C.; Arey, B.; Autrey, T.; Kauzlarich, S. M. *J. Phys. Chem. C* **2008**, *113*, 1098.
- Stephens, F. H.; Baker, R. T.; Matus, M. H.; Grant, D. J.; Dixon, D. A. *Angew. Chem., Int. Ed.* **2007**, *46*, 746.
- Xiong, Z. T.; Chua, Y. S.; Wu, G. T.; Xu, W. L.; Chen, P.; Shaw, W.; Karkamkar, A.; Linehan, J.; Smurthaite, T.; Autrey, T. *Chem. Commun.* **2008**, 5595.
- Xiong, Z. T.; Yong, C. K.; Wu, G. T.; Chen, P.; Shaw, W.; Karkamkar, A.; Autrey, T.; Jones, M. O.; Johnson, S. R.; Edwards, P. P.; David, W. I. F. *Nat. Mater.* **2008**, *7*, 138.
- Wang, P.; Orimo, S.; Tanabe, K.; Fujii, H. *J. Alloys Compd.* **2003**, *350*, 218.
- Wu, H.; Zhou, W.; Yildirim, T. *J. Am. Chem. Soc.* **2008**, *130*, 14834.
- Wu, C.; Wu, G.; Xiong, Z.; David, W. I. F.; Ryan, K. R.; Jones, M. O.; Edwards, P. P.; Chu, H.; Chen, P. *Inorg. Chem.* **2010**, *49*, 4319.
- Luedtke, A. T.; Autrey, T. *Inorg. Chem.* **2010**, *49*, 3905.
- Xiong, Z. T.; Wu, G. T.; Chua, Y. S.; Hu, J. J.; He, T.; Xu, W. L.; Chen, P. *Energy Environ. Sci.* **2008**, *1*, 360.
- Spielmann, J.; Jansen, G.; Bandmann, H.; Harder, S. *Angew. Chem., Int. Ed.* **2008**, *47*, 6290.
- Himashinie, V. K.; Diyabalanage, R. P. S.; Semelsberger, T. A.; Scott, B. L.; Bowden, M. E.; Davis, B. L.; Burrell, A. K. *Angew. Chem., Int. Ed.* **2007**, *46*, 8995.
- Kim, D. Y.; Singh, N. J.; Lee, H. M.; Kim, K. S. *Chem.—Eur. J.* **2009**, *15*, 5598.
- Lee, S. M.; Kang, X. D.; Wang, P.; Cheng, H. M.; Lee, Y. H. *ChemPhysChem* **2009**, *10*, 1825.
- Ramzan, M.; Silveary, F.; Blomqvist, A.; Scheicher, R. H.; Lebegue, S.; Ahuja, R. *Phys. Rev. B* **2009**, *79*, 132102.
- Wu, C.; Wu, G.; Xiong, Z.; Han, X.; Chu, H.; He, T.; Chen, P. *Chem. Mater.* **2009**, *22*, 3.
- West, D.; Limpijumnong, S.; Zhang, S. B. *Phys. Rev. B* **2009**, *80*, 064109.
- Kathmann, S. M.; Parvanov, V.; Schenter, G. K.; Stowe, A. C.; Daemen, L. L.; Hartl, M.; Linehan, J.; Hess, N. J.; Karkamkar, A.; Autrey, T. *J. Chem. Phys.* **2009**, *130*.
- Staubitz, A.; Besora, M.; Harvey, J. N.; Manners, I. *Inorg. Chem.* **2008**, *47*, 5910.
- Nguyen, V. S.; Matus, M. H.; Grant, D. J.; Nguyen, M. T.; Dixon, D. A. *J. Phys. Chem. A* **2007**, *111*, 8844.
- Miranda, C. R.; Ceder, G. *J. Chem. Phys.* **2007**, *126*.
- Zhang, J.; Zhang, S.; Li, Q. S. *J. Mol. Struct.: THEOCHEM* **2005**, *717*, 33.
- Li, Q. S.; Zhang, J.; Zhang, S. *Chem. Phys. Lett.* **2005**, *404*, 100.
- Morrison, C. A.; Siddick, M. M. *Angew. Chem., Int. Ed.* **2004**, *43*, 4780.
- Pons, V.; Baker, R. T.; Szyszczak, N. K.; Heldebrant, D. J.; Linehan, J. C.; Matus, M. H.; Grant, D. J.; Dixon, D. A. *Chem. Commun.* **2008**, 6597.
- Lee, T. B.; McKee, M. L. *Inorg. Chem.* **2009**, *48*, 7564.
- Ramzan, M.; Silveary, F.; Blomqvist, A.; Scheicher, R. H.; Lebegue, S.; Ahuja, R. *Phys. Rev. B* **2009**, *79*.
- Swinnen, S.; Nguyen, V. S.; Nguyen, M. T. *Chem. Phys. Lett.* **2010**, *489*, 148.

- (34) Kohn, W.; Sham, L. J. *Phys. Rev.* **1965**, *140*, A1133.  
(35) Blöchl, P. E. *Phys. Rev. B* **1994**, *50*, 17953.  
(36) Perdew, J. P.; Wang, Y. *Phys. Rev. B* **1992**, *45*, 13244.  
(37) Kresse, G.; Furthmüller, J. *Phys. Rev. B* **1996**, *54*, 11169.  
(38) Monkhorst, H. J.; Pack, J. D. *Phys. Rev. B* **1976**, *13*, 5188.  
(39) Becke, A. D.; Edgecombe, K. E. *J. Chem. Phys.* **1990**, *92*, 5397.  
(40) Blöchl, P. E.; Jepsen, O.; Andersen, O. K. *Phys. Rev. B* **1994**, *49*, 16223.  
(41) Wagner, F. R. <http://www.cpfms.mpg.de/ELF/index.php?content=02topol.txt>, 2002.  
(42) Zhang, C.; Alavi, A. *J. Phys. Chem. B* **2006**, *110*, 7139.  
(43) Shaw, W. J.; Linehan, J. C.; Szymczak, N. K.; Heldebrant, D. J.; Yonker, C.; Camaioni, D. M.; Baker, R. T.; Autrey, T. *Angew. Chem., Int. Ed.* **2008**, *47*, 7493.  
(44) Bowden, M. E.; Gainsford, G. J.; Robinson, W. T. *Aust. J. Chem.* **2007**, *60*, 149.  
(45) Richardson, T.; de Gala, S.; Crabtree, R. H.; Siegbahn, P. E. M. *J. Am. Chem. Soc.* **1995**, *117*, 12875.

JP103708Z